Proc. Natl. Acad. Sci. USA
Vol. 89, pp. 9855–9859, October 1992
Biophysics

Growing tips of type I collagen fibrils formed *in vitro* are near-paraboloidal in shape, implying a reciprocal relationship between accretion and diameter

D. F. HOLMES*, J. A. CHAPMAN*, D. J. PROCKOP†, AND K. E. KADLER*‡

*Departments of Biochemistry/Molecular Biology and Medical Biophysics, University of Manchester Medical School, Oxford Road, Manchester M13 9PT, United Kingdom; and †Department of Biochemistry and Molecular Biology, Jefferson Institute of Molecular Medicine, Jefferson Medical College, Bluemle Life Sciences Building, 233 South 10th Street, Philadelphia, PA 19107-5541

Contributed by D. J. Prockop, July 10, 1992

ABSTRACT **Collagen fibrils generated *in vitro* at 37°C by enzymic removal of C-terminal propeptides from type I pC-collagen (an intermediate in the normal processing of type I procollagen to collagen containing the C-terminal propeptides but not the N-terminal propeptides) display shape polarity, with one tip fine tapered and the other coarse tapered. Mass measurements by scanning transmission electron microscopy show that the mass per unit length along both kinds of tip increases roughly linearly over distances of ≈100 *D* periods from the fibril end [*D* (axial periodicity) = 67 nm]. The fine tips of fibrils of widely differing lengths exhibit near-identical mass distributions, the mass in all cases increasing at the rate of ≈17 molecules per *D* period, irrespective of fibril length. Coarse tips display less regular behavior. These results show that (*i*) the shape of a fine tip is not conical but resembles more closely a paraboloid of revolution, and (*ii*) for this shape to be maintained throughout growth, accretion (rate of mass uptake per unit area) cannot everywhere be the same on the surface of the tip but must decrease as the diameter increases. To a first approximation, accretion ∝ (diameter)$^{-1}$.**

How size and form are regulated in growing supramolecular assemblies is ill-understood. Such regulation is evident in the growth *in vivo* of certain fibrous assemblies, notably of interstitial collagen fibrils consisting predominantly of type I collagen. Although fibrils are indeterminate in length and have diameters in a broad range (10–500 nm, depending on age and tissue), individual fibrils tend to be fairly uniform in diameter, except at their growing ends. Moreover, bundles of newly formed fibrils in young tissues frequently exhibit sharp diameter distributions (1). Reconstitution of collagen monomers into fibrils *in vitro* leads to broader diameter distributions but accretion still occurs, mainly at ends, generating the characteristic fibrillar shape (2). Collagen fibrillogenesis *in vitro* is a classic example of an entropy-driven self-assembly process in which the information needed to form the highly elongated *D*-periodic fibrils [*D* (axial periodicity) = 67 nm before dehydration] is intrinsic to the collagen molecule (3). It is clear that this information must also specify some basic control of shape during self-assembly. The quantitative findings presented here are relevant to this shape-determining mechanism in collagen fibrillogenesis.

Studies of the early development of shape can be made on fibril ends. A suitable fibril-forming system has been developed by Kadler *et al.* (3, 4). Enzymic removal of C-terminal propeptides from type I pC-collagen (an intermediate in the normal processing of type I procollagen to collagen containing the C- but not the N-terminal propeptides) generates fibrils *in vitro* under near-physiological conditions. Fibrils formed between 29°C and 34°C, large enough to be observable by light microscopy, were found to have a pointed end and a blunt end, with growth occurring only from pointed ends; any growth at a blunt end took the form of a spear-like projection, which then acted as a new pointed tip for oppositely directed growth (5). Quantitative electron-optical measurements on narrower fibrils, formed at 37°C and resembling those formed *in vivo*, are not readily made by conventional procedures. Instead, we have used scanning transmission electron microscopy (STEM) to map the axial distribution of mass along growing tips. The results point to a growth mechanism in which accretion onto a tip surface (rate of mass uptake per unit area) decreases as the local diameter increases.

MATERIALS AND METHODS

Source of Materials. ^{14}C-labeled L-amino acids were from ICN, fertile hen eggs were from Northern Biological Supplies (St. Annes-on-Sea, U.K.), and carbon rods were from Agar Scientific (Stanstead, U.K.). Water used was from a Milli-Q Plus (Millipore) purification system.

Preparation of Procollagen and pC-Collagen. ^{14}C-labeled type I procollagen was purified from the medium of cultured human dermal fibroblasts in culture (3). Procollagen concentration was determined by colorimetric hydroxyproline analysis (6), assuming 10.1% hydroxyproline by weight for type I procollagen (7). The type I pC-collagen was prepared by digesting the type I procollagen with partially purified procollagen N-terminal proteinase (8) and then purified by gel filtration (3).

Fibril Formation. Fibril formation was initiated as described (3) by incubating pC-collagen (50 μg/ml) with procollagen C-terminal proteinase (9) (50 units/ml) at 37°C. One unit of activity was defined as the amount required to cleave 1 μg of type I procollagen in 1 h at 34°C in a reaction system containing type I procollagen (12 μg/ml). In brief, pC-collagen and C-terminal proteinase in a fibril-formation buffer (for composition see ref. 3) were added to a 1.5-ml microcentrifuge tube and the tube was charged with water-saturated 5% CO_2/95% air.

Electron Microscopy. Unstained fibrils were collected on carbon-filmed 600-mesh copper grids (Gilder, Grantham, U.K.). A drop of the incubated sample was left on the grid for 15 s; the grid was then flushed with 4 drops of water and allowed to air-dry. Some grids were rotary-shadowed with platinum at an angle of 4°.

A JEOL 1200EX, operating at 120 kV, was used for conventional transmission electron microscopy (TEM) and also, in combination with the ASID10 scanning attachment,

The publication costs of this article were defrayed in part by page charge payment. This article must therefore be hereby marked "*advertisement*" in accordance with 18 U.S.C. §1734 solely to indicate this fact.

Abbreviations: AMD, axial mass distribution; STEM, scanning transmission electron microscopy; TEM, conventional transmission electron microscopy.

‡To whom reprint requests should be addressed.

for STEM. For operation in the STEM mode, the instrument was equipped with an external digital scan control and a digital data acquisition system (10). The annular dark-field detector, of the scintillator/photomultiplier type, had a collection angle ranging from 25 to 75 milliradians.

Micrographs for mass-per-unit-length measurements were taken at an instrumental magnification of ×10,000 or ×20,000 (pixel sizes, 21.2 and 10.6 nm, respectively); the defocused spot size on the specimen was close to the pixel size in each case. The electron dose was <100 e·nm^{-2}, well within the limit for negligible mass loss from protein at an accelerating voltage of 120 kV (11). All mass measurements used tobacco mosaic virus as a comparative standard [mass per unit length, 131 kDa·nm^{-1} (12)]; procedures were the same as those used with dedicated field emission STEM instruments (11). The signal from the dark-field detector was linearly dependent on the mass per unit area of carbon films up to 50 kDa·nm^{-2}. The greatest mass thickness measured on unstained fibrils was within this limit. A diffraction grating replica (2160 lines per mm) was used for magnification calibration.

RESULTS

Morphology of Fibrils. Fig. 1 shows unstained fibrils formed in the cell-free processing system. The image was recorded by bright-field TEM at low magnification with minimal electron exposure (10 e·nm^{-2}). These fibrils are typical of those subsequently analyzed by quantitative dark-field STEM (see below). A complete fibril, ≈100 μm long but partly obscured by two bars of the supporting grid, appears in the upper part of the image. Three domains are distinguishable: a finely pointed tip (labeled α), a central region of apparently uniform diameter (the shaft) and, at the other end, a coarser tip (labeled β). This shape polarity, with distinct fine and coarse tips, was a characteristic feature of fibrils having both ends visible. Fibrils tended to associate in clusters in which outwardly directed fine tips predominated, suggesting that most growth has occurred at the fine tips. Spear-like projections, similar to those formed at lower temperatures and observed by light microscopy (5), were not found.

Molecular Polarity of Tips. Fig. 2 shows, at higher magnification, the two ends of a fibril contrasted by rotary shadowing and viewed by TEM. Fibrils prepared in this way revealed, within each *D* period, a distribution of shadowing intensity that was clearly polarized in axial direction. Comparison with fibrils positively stained with uranyl acetate and lightly shadowed (data not shown) allowed the molecular polarity in the staining pattern to be related to the intraperiod polarity after rotary shadowing. This established the molecular polarities at the two shadowed tips. Surprisingly, at both tips, fine and coarse, collagen molecules were oriented with their N termini closest to the nearby fibril end (compare Fig. 2 *A* and *B*), implying a switch in molecular polarity somewhere within the fibril. This switch in direction was not invariable. About 10% of fibrils had a normal fine-pointed tip but an abnormal blunt, irregular end with a frayed appearance (data not shown). Positive staining of these frayed ends indicated that the collagen molecules here were oriented with their C termini closest to the end of the fibril.

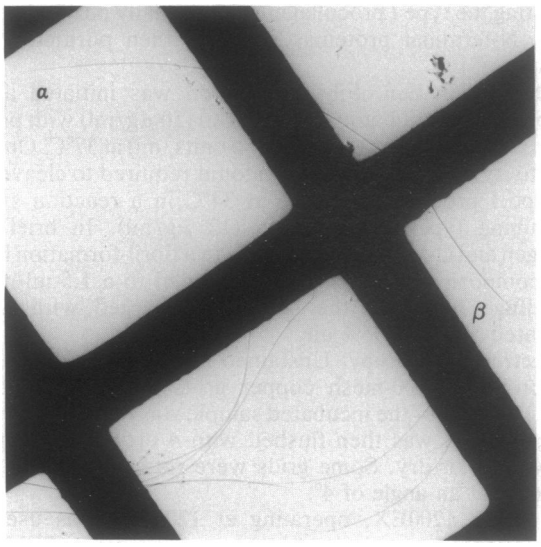

FIG. 1. Unstained collagen fibrils on a carbon-filmed supporting grid, imaged at low magnification and low electron exposure in the bright-field TEM mode. A complete fibril, 100 μm long and crossing two grid bars, is labeled α at its fine tip and β at its coarse tip. The scale is indicated by the size of the open grid squares, which are 50 μm across. (×750.)

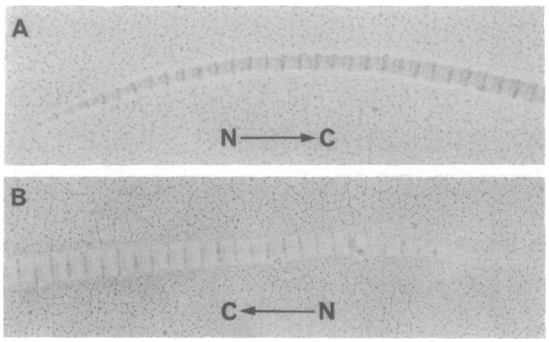

FIG. 2. TEM images of fibril tips after rotary shadowing with platinum. A typical fine tip is shown in *A* and a coarse tip is shown in *B*. Asymmetry in the intraperiod pattern allows the molecular polarity, N-terminal → C-terminal, to be established. The different polarities at the two tips imply a switch in molecular polarity somewhere within the fibril. The axial periodicity is ≈67 nm.

Mass Mapping of Tips. Typical dark-field STEM images of unstained tips appear in Fig. 3*A* (a fine tip) and Fig. 3*D* (a coarse tip). Mass data recorded over short lengths of fibril (≈15*D* in axial extent) are displayed in perspective form (Fig. 3 *B* and *E*). Single intensity scans transverse to (i.e., at right angles to) the fibril long axis generate a series of peaks; the area under each peak is a measure of the transverse mass of the fibril covered by the scan (adjoining scans are axially separated by ≈*D*/3). These perspective views show that the axial mass distribution along a fibril is fairly smooth, apart from a *D*-periodic variation arising from the fibril gap/overlap structure. The absence of marked irregularities across the fibril is consistent with the fibril having a circular (rather than irregular) cross-section. Further evidence that fibrils formed in this way are roughly circular in outline comes from sectioning studies (13).

Integration of image intensities from an integral number of *D* periods (usually 4) and calibration using tobacco mosaic virus as a mass standard (see *Materials and Methods*) enabled the mass per unit length of the fibril to be determined as a function of axial position along the fibril. We refer to this mass versus position plot as the axial mass distribution (AMD) of the fibril. Typical AMDs from fine and coarse tips are shown in Fig. 3 *C* and *F*, respectively. AMDs from fine tips (e.g., see Fig. 3*C*) were characteristically near-linear over ≈100 *D* periods (>20 molecular lengths of 300 nm). Coarse tips displayed less regular AMDs (Fig. 3*F*).

The superposition of AMD data from 6 fine tips in Fig. 4*A* shows that fine tips from different fibrils have near-identical mass profiles; not only is linearity common to all tips but the slope of each AMD varies little from one fibril to another, irrespective of fibril length. Fibrils visible in their entirety ranged in length from 55 to 240 μm (800–3500 *D* periods) but

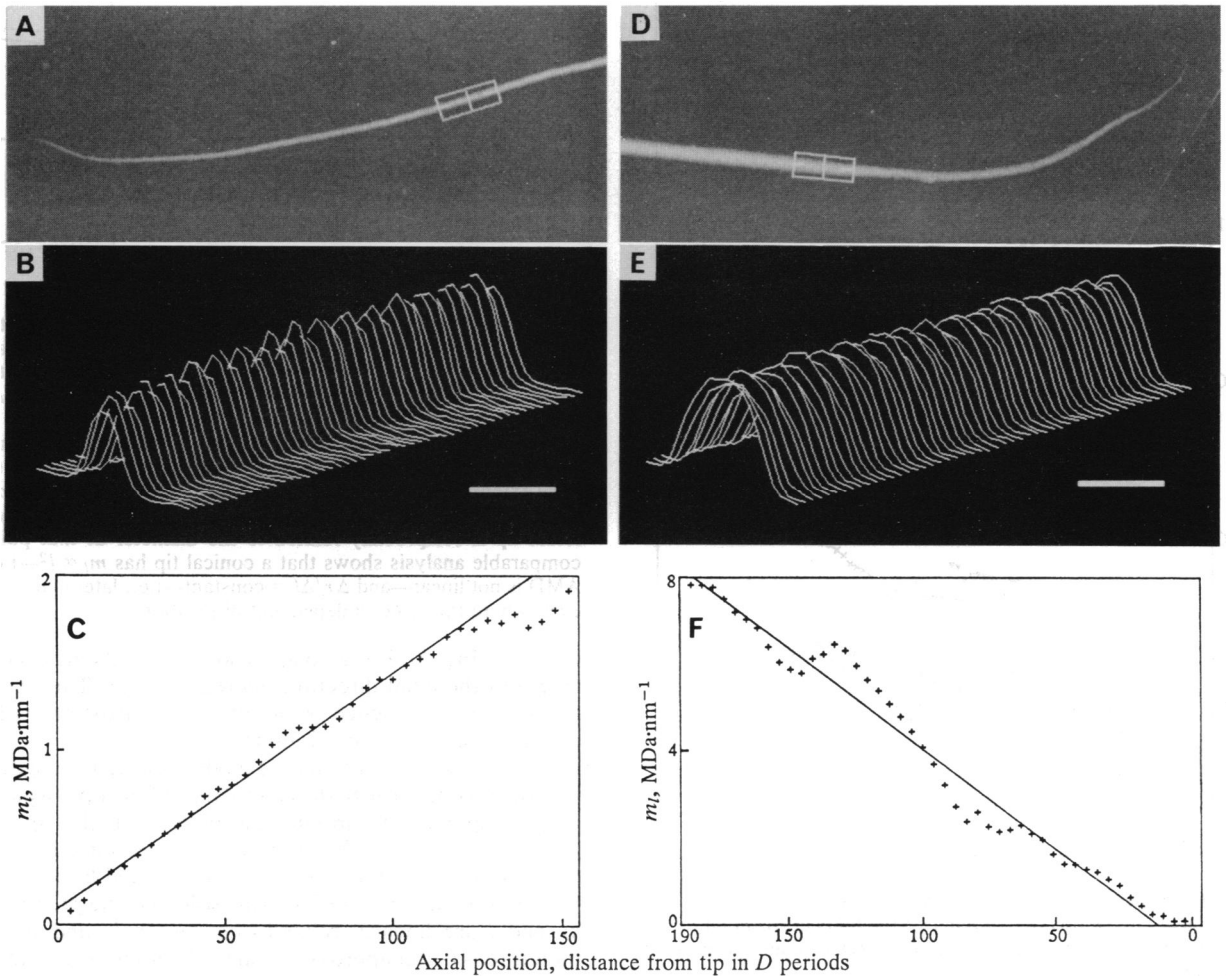

FIG. 3. (*A–C*) Data from a fine tip of a fibril. (*D–F*) Data from the coarse tip of the same fibril. (*A* and *D*) Dark-field STEM images; each boxed region has an axial length of 1 μm and a breadth of 0.4 μm. (*B* and *E*) Perspective displays of scans from the entire boxed regions; an individual scan shows the transverse distribution of mass across the fibril; adjoining scans are separated axially by $D/3$. The smoothness and symmetry of the scans are consistent with the tips being roughly circular in transverse section. In *B* and *E* the magnifications in the two horizontal directions are ×55,000; the vertical scale is arbitrary. (*C* and *F*) AMDs obtained from integrated intensity measurements on the STEM images shown in *A* and *D*. Each point is the m_l of the fibril averaged over 4 *D* periods. Solid lines are obtained by linear least-squares fits (excluding the last 7 points in *C* where systematic departure from linearity is apparent); vertical scales in *C* and *F* differ by a factor of 4. The overall length of the fibril was ≈150 μm—i.e., *C* and *F* are separated axially by ≈2000 *D* periods.

this had no effect on the AMDs of the fine tips. Coarse tips exhibited less regular mass distributions, with the mean slope varying from one tip to another by a factor of up to 3 (Fig. 4*B*); a tendency for the mean slopes of AMDs from coarse tips to increase with fibril length was noted. Table 1 summarizes AMD data from fine and coarse tips and reexpresses the incremental growth per *D* period in terms of numbers of molecules passing through tip cross-sections.

Although AMDs from fine tips were approximately linear over extended axial distances (≈100 *D* periods), all showed some decrease in slope as *l* (the distance from the tip end) increased and the central shaft of the fibril was approached. This is evident in Fig. 4*A* for values of $l/D > 120$. In a few instances, departures from linearity occurred in the immediate vicinity of the tip end. Of the 40 fine tips examined, 4 displayed a steeper slope in the first 10 *D* periods. These departures from linearity all had one feature in common; where they occurred, the slope always decreased with increasing distance from the end of the tip. Any overall curvature in the AMD was downward, never upward.

DISCUSSION

Shape polarity is not confined to collagen fibrils growing *in vitro*. Developing chick tendon fibrils, 7–15 μm long, have differing tapers at their two ends, with maximum diameters attained 1.6 μm from one end and 4.5 μm from the other; molecular polarities were not determined (15). The present study has shown that the two ends differ in fibrils growing in a cell-free system in which C-terminal propeptides are cleaved from type I pC-collagen. Their finely tapered ends all have similar mass profiles, whereas the coarse tips display much greater variability. The relative rates of growth of the two ends are not yet known but comparison with light-optical studies of larger fibrils formed at lower temperatures in the same system (5) suggests that growth predominates at the fine tips.

At these finely tapered tips, AMDs are near-linear for ≈100 *D* periods, all tips displaying much the same increment (≈17 molecules per *D* period) over this region, irrespective of fibril length (Table 1). A previous dark-field TEM study of collagen fibril growth *in vitro*, using acetic acid-extracted type I collagen (fully processed and partially cross-linked), also showed the tips of early fibrils to have roughly linear AMDs with slopes independent of fibril length (16). As in the present study, approximate linearity of the AMDs was confined to tip regions and slopes lessened as the central shaft of the fibril was approached.

It is evident from the AMD data and the absence of any dependence on fibril lengths that a growing fine tip must

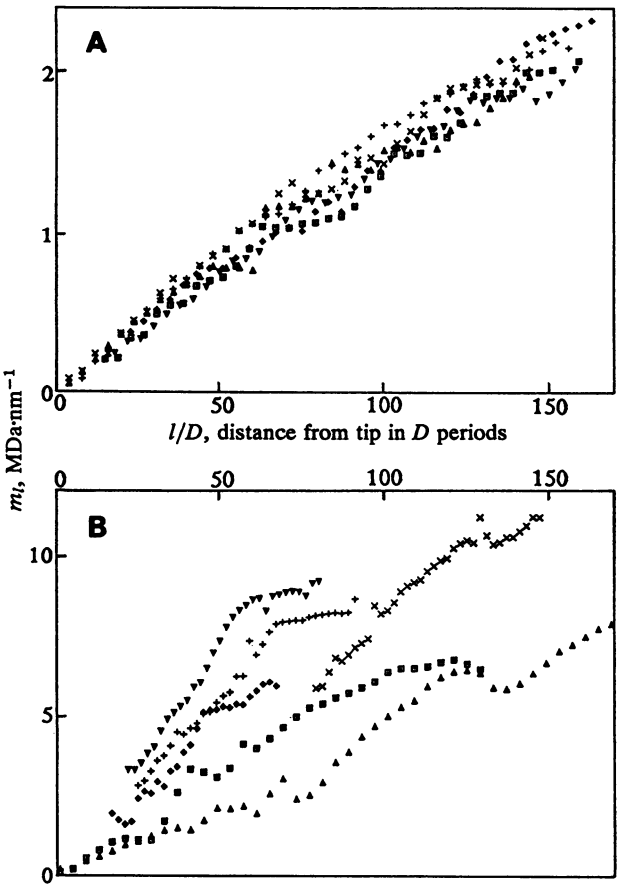

FIG. 4. Superposition of AMD data from 6 typical fine tips (*A*) and 6 typical coarse tips (*B*). Origins on the plots correspond to the ends of the fibrils. The range of m_l in *B* is greater than that in *A* by a factor of ≈5.

maintain a fairly constant shape as collagen monomers (or oligomers) accrete onto its surface. This shape and how it is maintained during accretion have hitherto received little attention. Accretion can here be treated simply as the rate at which additional mass accumulates on unit area of the surface, ignoring the nature of the accreting units. Our data preclude any determination of this rate as a function of time. Nevertheless, some information on relative rates of accretion at differing positions on the tip surface can be inferred. We note first that accretion cannot be the same everywhere on a tip surface, regardless of position. If, as available evidence suggests, tips are circular in cross-sectional outline, such growth would imply that the tip is conical in shape, its radius r increasing linearly with l, the distance from its apex (see

Table 1. m_l data from fine and coarse tips

	Increment growth per *D* period			
	Mean rate of increase in m_l per *D* period, kDa·nm^{-1}	Mean rate of increase in *N* per *D* period	SD, %	No. of samples
Fine tips	15	17	8	40
Coarse tips	98	113	31	14

The first column of numbers gives the mean slope of graphs in which m_l has been plotted against l/D, the distance from the tip in *D* periods. The second column reexpresses this in terms of *N*, the number of molecules intersecting a fibril cross-section (through an overlap zone). The relationship between m_l and *N* is given by $m_l = MN/5D$, where *M* is the mass of a collagen molecule (290 kDa) and molecules are mutually staggered by *D* (axial periodicity, 67 nm), or integral multiples thereof (14). It follows that $N = 1.15\ m_l$.

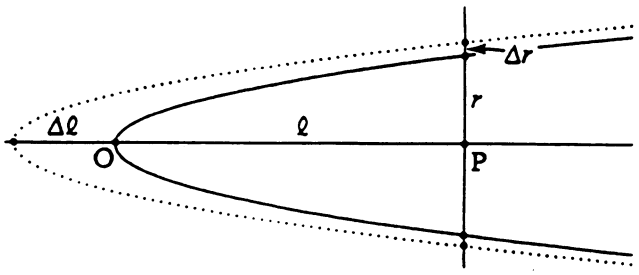

FIG. 5. Growth of a paraboloidal tip. Continuous curve represents a longitudinal section through the axis OP; at P, a distance l from the apex O, the radius is r. Dotted curve shows the tip a short interval of time, Δt, later. It is unchanged in shape but has extended axially by Δl and the radius at P has increased to $r + \Delta r$. As the section is a parabola, $r^2 = kl$ where k is a constant; $m_l = \rho\pi r^2$ where ρ is the tip density; hence $m_l \propto l$—i.e., a paraboloidal tip has a linear AMD. Lateral accretion can be expressed as $\rho\Delta r/\Delta t$, and the rate of axial extension of the tip apex is $\Delta l/\Delta t$. The ratio of the two = $\rho\Delta r/\Delta l = k\rho/2r$—i.e., lateral accretion at any point on a growing paraboloidal tip is reciprocally related to the diameter at that point. (A comparable analysis shows that a conical tip has $m_l \propto l^2$—i.e., the AMD is not linear—and $\Delta r/\Delta l$ = constant—i.e., lateral accretion is everywhere the same, independent of position.)

legend to Fig. 5). For a cone, however, m_l, its mass per unit length in the axial direction, increases as l^2. The observed near-linear dependence of m_l on l is inconsistent with this uniform-accretion conical model.

Fig. 5 presents an alternative model in which a longitudinal section passing through the central axis of the tip is a parabola with its apex at the tip end; the radius r of the tip is now proportional to $\sqrt{l}$. With transverse sections circular in outline, the three-dimensional solid bounded by the surface is a paraboloid of revolution. This solid has the property that m_l and l are linearly related—i.e., $m_l \propto l$—and it offers, therefore, a better approximation to observed AMD data than the conical model. This is confirmed in Fig. 6 where $\log_{10}(m_l)$ is plotted against $\log_{10}(l/D)$, using values of m_l and l measured on 6 fine tips; the slope of the log/log plot accords much more closely with that predicted by the paraboloidal model than with that predicted by a cone.

For the paraboloidal shape to remain unchanged during growth, accretion cannot be uniform over its surface. As

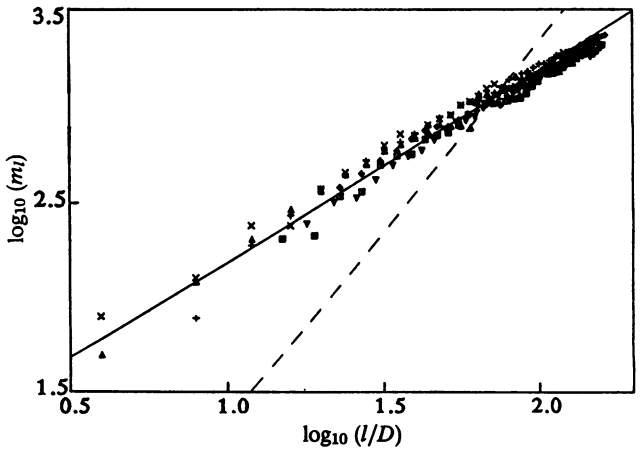

FIG. 6. Log/log plot of AMD data from Fig. 4*A* for fine tips. If $m_l = k(l/D)^p$, where k and p are constants, then $\log_{10}(m_l) = p\log_{10}(l/D) + \log_{10}k$. For a conical tip, $m_l \propto (l/D)^2$—i.e., $p = 2$; for a paraboloidal tip, $m_l \propto l/D$—i.e., $p = 1$ (see *Discussion*). Lines corresponding to $p = 1$ (solid line) and $p = 2$ (dashed line), each passing through the center of mass of the data, are shown superposed on the plot. The line corresponding to $p = 1$ is in good agreement with the data (a linear least-squares fit gives a slope of 0.95), in clear contrast to the $p = 2$ line.

indicated in the legend to Fig. 5, the ratio radial growth/axial elongation is inversely related to the radius r, implying that mass uptake per unit area is greatest at the tip apex and lessens as the tip grows in size. On an ideal paraboloidal surface, accretion at any point is reciprocally related to the diameter at that point. A collagen fibril tip is not an ideal paraboloid but the mass data leave little doubt that, for the first $\approx 100\ D$ periods, it is a much better approximation to the tip shape than a cone. Beyond this, the falloff in accretion with increasing diameter is even greater as the central shaft of the fibril is approached.

The molecular mechanism underlying this accretion behavior, seemingly a basic feature of collagen self-assembly favoring end growth of a fibril at the expense of growth elsewhere, is not yet understood. A possible mechanism is suggested by recent observations on fibrin fibers, indicating that twisting of fibers limits their radial growth (17). An earlier proposal along similar lines has been suggested for collagen (18); since then, evidence has accumulated pointing to a slow right-handed quaternary twisting in collagen fibrils (19). The possibility that this twisting may limit radial growth in collagen has now to be considered.

The authors are grateful to Dr. B. Brodsky, Dr. E. Eikenberry, and Dr. D. J. S. Hulmes for valuable criticisms. This work was supported by grants from the Wellcome Trust (to K.E.K. and to J.A.C.), the Arthritis and Rheumatism Council (to J.A.C. and D.F.H.), and the National Institutes of Health (AR38188 to D.J.P.). K.E.K. is recipient of a Senior Research Fellowship Award in Basic Biomedical Science from the Wellcome Trust.

1. Parry, D. A. D. & Craig, A. S. (1984) in *Ultrastructure of the Connective Tissue Matrix*, eds. Ruggeri, A. & Motta, P. M. (Nijhoff, Boston), pp. 34–64.
2. Bard, J. B. L. & Chapman, J. A. (1973) *Nature (London) New Biol.* **246**, 83–84.
3. Kadler, K. E., Hojima, Y. & Prockop, D. J. (1987) *J. Biol. Chem.* **262**, 15696–15701.
4. Kadler, K. E., Hulmes, D. J. S., Hojima, Y. & Prockop, D. J. (1990) *Ann. N.Y. Acad. Sci.* **580**, 214–224.
5. Kadler, K. E., Hojima, Y. & Prockop, D. J. (1990) *Biochem. J.* **268**, 339–343.
6. Woessner, J. F., Jr. (1961) *Arch. Biochem. Biophys.* **93**, 440–447.
7. Fiedler-Nagy, C., Bruckner, P., Hayashi, T. & Prockop, D. J. (1981) *Arch. Biochem. Biophys.* **212**, 668–677.
8. Hojima, Y., McKenzie, J., van der Rest, M. & Prockop, D. J. (1989) *J. Biol. Chem.* **264**, 11336–11345.
9. Hojima, Y., van der Rest, M. & Prockop, D. J. (1985) *J. Biol. Chem.* **260**, 15996–16003.
10. Holmes, D. F., Mould, A. P. & Chapman, J. A. (1991) *J. Mol. Biol.* **220**, 111–123.
11. Engel, A. (1982) *Micron* **13**, 425–436.
12. Kaper, J. M. (1986) in *Molecular Basis of Virology*, ed. Fraenkel-Conrat, H. (Van Nostrand Reinhold, New York), pp. 1–133.
13. Hulmes, D. J. S., Kadler, K. E., Mould, A. P., Hojima, Y., Holmes, D. F., Cummings, C., Chapman, J. A. & Prockop, D. J. (1989) *J. Mol. Biol.* **210**, 337–345.
14. Chapman, J. A. & Hulmes, D. J. S. (1984) in *Ultrastructure of the Connective Tissue Matrix*, eds. Ruggeri, A. & Motta, P. M. (Nijhoff, Boston), pp. 1–33.
15. Birk, D. E., Zycband, E. I., Winkelmann, D. E. & Trelstad, R. L. (1989) *Proc. Natl. Acad. Sci. USA* **86**, 4549–4553.
16. Holmes, D. F. & Chapman, J. A. (1979) *Biochem. Biophys. Res. Commun.* **87**, 993–999.
17. Weisel, J. W., Nagaswami, C. & Makowski, L. (1987) *Proc. Natl. Acad. Sci. USA* **84**, 8991–8995.
18. Chapman, J. A. (1965) in *CIBA Foundation Symposium: Principles of Biomolecular Organization*, eds. Wolstenholme, G. & O'Connor, M. (Churchill, London), pp. 129–130.
19. Chapman, J. A. (1984) in *Connective Tissue Matrix*, ed. Hukins, D. W. L. (Macmillan, London), pp. 89–132.